Photophysics of Organic Photostabilizers. Ab Initio Study of the Excited-State Deactivation Mechanisms of 2-(2′-Hydroxyphenyl)benzotriazole

Andrzej L. Sobolewski,*,† Wolfgang Domcke,‡ and Christof Hättig§

Institute of Physics, Polish Academy of Sciences, PL-02668 Warsaw, Poland, Department of Chemistry, Technical University of Munich, D-85747 Garching, Germany, and Institute of Nanotechnology, Forschungszentrum Karlsruhe, D-76021 Karlsruhe, Germany

Excited-state reaction paths and the corresponding energy profiles of 2-(2′-hydroxyphenyl)benzotriazole (TIN−H) have been determined with the CC2 (simplified singles-and-doubles coupled-cluster) ab initio method. Hydrogen transfer along the intramolecular hydrogen bond, torsion of the aromatic rings and pyramidization of the central nitrogen atom are identified as the most relevant photochemical reaction coordinates. The keto-type planar S_1 state reached by barrierless intramolecular hydrogen transfer is found to be unstable with respect to torsion. The latter mode, together with a moderate pyramidization of the central nitrogen atom, provides barrierless access to a S_1−S_0 conical intersection. Only the π-type orbitals of the aromatic rings are involved in the open-shell structures. The S_1−S_0 conical intersection, which occurs for perpendicular geometry of the aromatic rings, is a pure biradical. From the conical intersection, a barrierless reaction path steers the system back to the enol-type minimum of the S_0 potential-energy surface, thus closing the photocycle. This photophysical pathway accounts for the remarkable photostability of the molecule.

1. Introduction

The spectroscopy and photophysics of 2-(2′-hydroxyphenyl)-benzotriazole (Tinuvin or TIN−H, see Scheme 1) and its 5′-methylated derivative (TIN−P) have extensively been studied, because these compounds are particularly efficient UV stabi-lizers.[1−6] More than 99.9% of the light energy absorbed in the $S_0 \rightarrow S_1$ transition of TIN−P is dissipated as heat.[6]

Extensive investigations of the fluorescence properties of TIN−P and related compounds in various environments have led to the conclusion that the intramolecular hydrogen bond is of fundamental importance for their function as photostabilizers,[3−8] although this interpretation has occasionally been disputed.[9] Picosecond and femtosecond pump−probe measurements per-formed since the early 1990s have revealed the intrinsic time scales of the excited-state intramolecular hydrogen-transfer (ESIHT) process ($\approx$100 fs), the radiationless decay of the excited keto form ($\approx$150 fs) as well as the hydrogen back-transfer in the electronic ground state ($\approx$600 fs).[10−13] One of the remarkable features of TIN−P is the extremely rapid depopulation of the lowest excited singlet state of the keto form (S_1'). It is orders of magnitude faster than that of related intramolecularly hydrogen-bonded aromatics such as 2-(2′-hydroxyphenyl)benzoxazole (HBO) or 2-(2′-hydroxyphenyl)-benzothiazole (HBT).[6,7]

While there is rather broad consensus on the essential role of the barrierless ESIHT process in TIN and related photosta-bilizers, the specific mechanisms which are responsible for the ultrafast deactivation of the S_1' state of TIN−P are still largely unknown. It has been argued that the strongly reduced S_1'−S_0' energy gap (by about 10^4 cm^{-1}) can account for enhanced radiationless decay according to the energy-gap law.[14] The

SCHEME 1

R=H: TIN−H

R=CH₃: TIN−P
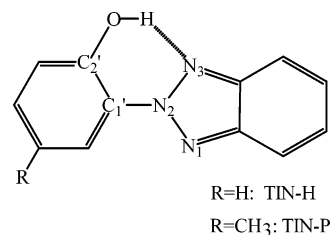
finding that the S_1' radiationless decay rate of TIN−P exhibits a pronounced temperature dependence in low-temperature organic glasses has been considered as evidence that large-amplitude torsional motion of the aromatic rings may be essential for the decay process.[15] Further evidence for an interplay of hydrogen transfer and twisting (formation of twisted intramolecular charge-transfer (TICT) states) has been obtained by the investigation of the fluorescence properties of pretwisted (by steric hindrance of methyl substituents) derivatives of TIN.[16] Time-resolved resonance Raman studies, on the other hand, have provided evidence that low-frequency in-plane modes associated with the proton-transfer process serve as major accepting modes of the internal-conversion process.[17]

While many computational studies have been concerned with the reaction mechanism of ESIHT systems (for reviews, see, e.g., refs 18 and 19), very few calculations have so far been performed for hydroxyphenyl−benzotriazole derivatives because of their considerable size. The ground-state equilibrium geom-etry of TIN−P has been determined at the level of second-order Møller−Plesset perturbation theory (MP2) by Catalan et al.[20] Estevez et al. have performed single-point complete-active-space self-consistent-field (CASSCF) calculations for a computation-ally more tractable fragment of TIN−H (2-(2′-hydroxyphenyl)-triazole, deleting the fused benzene ring; see Scheme 1).[21] They emphasized the relevance of pyramidization at the N_2 atom (see Scheme 1) for the decrease of the S_1'−S_0' energy gap. For an

---

* Corresponding author. E-mail: sobola@ifpan.edu.pl
† Institute of Physics, Polish Academy of Sciences.
‡ Department of Chemistry, Technical University of Munich.
§ Institute of Nanotechnology, Forschungszentrum Karlsruhe.

additionally truncated subsystem, they were able to locate a $S_1'-S_0'$ conical intersection at the CASSCF level[21] which may serve as the funnel for an ultrafast $S_1' \rightarrow S_0$ internal conversion process.[22] More recently, Paterson et al. have performed a more exhaustive CASSCF study of the same model system (2-(2'-hydroxyphenyl)triazole).[23] These calculations indicated a $^1\pi\pi^*-{}^1n\pi^*$ state switch along the proton-transfer coordinate. This finding most likely is a consequence of the truncation of the molecule: the $^1\pi\pi^*$ states of the triazole five-membered ring are considerably higher in energy than those of the benzotriazole system. A conical intersection of the lowest $^1n\pi^*$ state with the S_0 state has been found for the 90° twisted configuration, thus providing computational evidence for the relevance of the TICT phenomenon in TIN.[23] In addition, the prefulvenic distortion of the phenyl ring[24-30] has been discussed as a reaction path for internal conversion through a conical intersection.[23] The latter mechanism is, however, generic for aromatic or heteroaromatic six-membered rings[24-30] and thus does not explain the exceptional photostability of TIN.

In the present work, we have applied the recently developed CC2 method,[31,32] which is a simplified and computationally efficient variant of coupled-cluster theory with single and double excitations, for a systematic exploration of the excited-state and ground-state potential-energy surfaces of TIN—H; see Scheme 1. To our knowledge, this is the first ab initio computational study of the excited-state energy surfaces of a hydroxyphenyl—benzotriazole compound.

2. Computational Methods

The ground-state equilibrium geometries of the hydrogen-bonded (enol) and open forms of TIN—H have been determined with the MP2 method. Excitation energies and response properties have been calculated with the CC2 method.[31,32] CC2 can be considered as the equivalent of MP2 for excited electronic states. The equilibrium geometries and reaction paths of the lowest excited singlet state of the system have been determined at the CC2 level, making use of the recently implemented analytic CC2 gradients.[33,34] To allow cost-effective calculations on the system of this size, the standard split-valence double-ζ basis set of TURBOMOLE[35] with polarization functions on heavy atoms (SV(P))[36] has been employed in these MP2 and CC2 calculations. The CC2 method has previously been used to characterize proton-transfer reaction paths of small ESIHT systems.[37] It has been shown in ref 37, by comparison with accurate CASPT2 and MR-AQCC data, that CC2 predicts qualitatively reliable energy profiles of excited-state proton-transfer reactions also in difficult cases where dynamical electron-correlation effects are of decisive importance.

Two excited-state reaction paths have been studied: the transfer of the hydrogen atom along the intramolecular hydrogen bond and the torsion of the phenolic ring against the triazole ring. The driving coordinate for the hydrogen-transfer reaction path is the OH distance of the phenolic hydroxy group. For the torsional reaction path, the $C_2'C_1'N_2N_1$ dihedral angle (see Scheme 1) has been chosen as the driving coordinate. All other nuclear degrees of freedom have been optimized for a given value of the driving coordinate, unless specified otherwise.

While CC2 is the method of choice for the exploration of photochemically relevant excited-state minimum-energy reaction paths, it is not appropriate for the characterization of the potential-energy surfaces in the immediate vicinity of conical intersections of the S_1 surface with the S_0 surface. The conical intersection between the S_1 and S_0 energy surfaces has therefore been located at the CASSCF level, using the corresponding
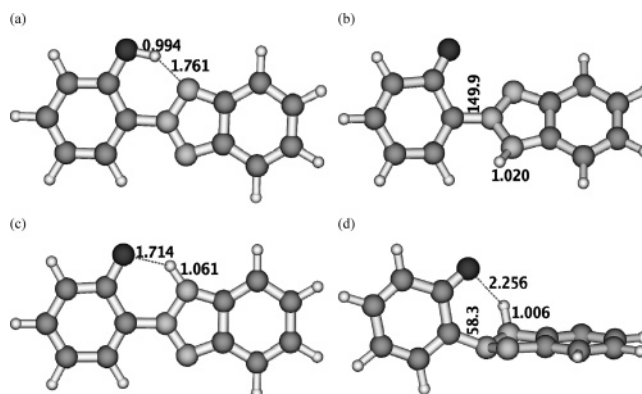

Figure 1. Equilibrium geometries of the stable structures of TIN—H in the electronic ground state (a and b) and distinguished structures of the system in the lowest excited singlet state: the metastable planar keto configuration (c) and the S_1-S_0 conical intersection (d). The numbers give the lengths of distinguished bonds (in Å) and the value of the inter-ring dihedral angle (in degrees).

module of the GAUSSIAN 98 program package.[38] The active space for the CASSCF calculations consisted of six electrons distributed over six π orbitals (the three highest occupied and three lowest unoccupied orbitals) determined by a restricted Hartree—Fock calculation at a guessed geometry of the conical intersection. The standard split-valence double-ζ basis set of GAUSSIAN with polarization functions on heavy atoms (6-31G*), which is essentially equivalent to the SV(P) basis set of TURBOMOLE, was employed in these CASSCF calculations. At the conical intersection, the system is an essentially pure biradical, that is, only two orbitals are singly occupied, while all other orbitals have occupation numbers very close to 0 or 2. This justifies the use of a rather compact (6 orbitals/6 electrons) active space in the CASSCF calculations.

All MP2 and CC2 calculations were carried out with the TURBOMOLE program package,[35] making use of the resolution-of-the-identity (RI) approximation for the evaluation of the electron-repulsion integrals.[39] To improve the accuracy of the spectroscopic data, the single-point energies and spectroscopic properties have been recalculated with Dunning's correlation-consistent basis set of double-ζ quality with polarization functions on all atoms (cc-pVDZ).[40] At the most crucial points of the energy hypersurfaces, additional single-point CC2 calculations have been performed with the cc-pVTZ triple-ζ basis set.

3. Results and Discussion

3.1. Ground-State Equilibrium Structures and Vertical Electronic Excitation Energies. Two local minima of TIN—H were found in unconstrained MP2 optimizations of the ground state. These are shown in Figure 1, parts a and b, with the most crucial geometry parameters indicated. The Cartesian geometry parameters of the structures are given in the Supporting Information. The global minimum (Figure 1a) represents the enol-like tautomer of TIN—H exhibiting a strong intramolecular hydrogen bond between the phenolic hydrogen and the nitrogen atom of the triazole ring. The two rings are coplanar at the enol minimum, and the system processes C_s symmetry.

Apparently, the coplanar keto tautomer (with the hydrogen attached to the triazole ring) does not represent a stable minimum at the MP2/SV(P) level. Any attempt of unconstrained optimization of this form restored the enol minimum. On the other hand, the open form of the keto tautomer, with the rings twisted by about 150° (Figure 1b), represents a second local

Photophysics of Organic Photostabilizers

J. Phys. Chem. A, Vol. 110, No. 19, 2006   **6303**

TABLE 1: Energy (ΔE), Oscillator Strength (f), and Dipole Moment (μ) of 2-(2′-Hydroxyphenyl)benzotriazole Calculated at the Crucial Points of the Potential-Energy Surfaces with the CC2/cc-pVTZ Method

state	ΔE/eV	f	μ/D
	Enol Closed-Form Minimum in the S_0 State		
S_0	0.0^a		1.47
$S_1(\pi\pi^*)$	4.01^b	0.44	4.11
$S_2(\pi\pi^*)$	4.62^b	0.13	0.53
$S_3(n\pi^*)$	5.55^b	0.0001	0.92
	Keto Open-Form Minimum in the S_0 State		
S_0	1.99^a		6.76
$S_1(\pi\pi^*)$	2.24^b	0.22	3.86
$S_2(\pi\pi^*)$	2.59^b	0.31	3.14
	Keto Closed-Form C_s Transient in the S_1 State		
S_0	2.04^c	0.32	4.64
$S_1(\pi\pi^*)$	3.21^a		2.60
	S_1–S_0 CASSCF Conical Intersection		
S_0	3.06^a		4.86
$S_1(\pi\pi^*)$	3.10^a		5.86
	S_1–S_0 CC2 Intersection		
S_0	2.65^a		3.37
$S_1(\pi\pi^*)$	2.75^a		7.22

^{a} Energy relative to the ground-state global minimum. ^{b} Vertical absorption. ^{c} Vertical fluorescence.

minimum of the S_0 energy surface. At the CC2/SV(P) level, the open keto form lies 1.99 eV above the global minimum. This energy difference appears to be saturated with respect to the basis set, since CC2/cc-pVDZ and CC2/cc-pVTZ calculations (see Table 1) yield very similar values. The open keto minimum is separated by a barrier of 0.24 eV (5.5 kcal/mol) from the closed enol minimum (CC2/cc-pVDZ value).

Vertical excitation energies and oscillator strengths of the two ground-state isomers of TIN—H are collected in Table 1. The enol form absorbs strongly ($f = 0.44$) in the UV ($\Delta E = 4.01$ eV), as expected for a good photostabilizer. The $S_1(\pi\pi^*)$ vertical excitation energy of the open keto form is strongly red-shifted ($\Delta E = 2.24$ eV) and the S_1–S_0 oscillator strength is smaller ($f = 0.22$). The lowest $^1n\pi^*$ state of TIN—H is much higher in energy than the lowest $^1\pi\pi^*$ state, as expected for an aromatic system of this size.

We are not aware of any gas-phase experimental data for TIN—H which we can compare to our calculated values. The only experimental data which we can refer to is the absorption spectrum of TIN—P (X = CH$_3$) obtained in cyclohexane (see ref 13 and references therein). The position of the maximum of the $S_0 \rightarrow S_1$ absorption profile has been estimated to be about 3.7 eV. The difference of 0.3 eV from the calculated value (4.0 eV) is well within the expected precision of the computational method and the expected difference between TIN—H and TIN—P.

An interesting conclusion results from the inspection of the dipole moments of the S_0 and S_1 states of the two isomers, collected in Table 1. The dipole moment of excited singlet state of the enol conformer (4.11 D) is more than twice as large as that of the ground state (1.47 D). The reverse is true for the keto tautomer: here the S_0 state is considerably more polar (6.76 D) than the S_1 state (3.86 D). These substantial variations of the dipole moment with tautomers and electronic state are expected to result in a significant red-shift (blue-shift) of the absorption spectrum of the enol (keto) form in polar environments.

3.2. Excited-State Minima and Conical Intersections. Optimization of the S_1 state with C_s symmetry constraint, starting from the equilibrium geometry of the ground state,

resulted in the structure shown in Figure 1c (the Cartesian geometry parameters are given in the Supporting Information). This structure represents a saddle point on the potential-energy surface of the S_1 state; it is unstable with respect to out-of-plane deformation. An unconstrained optimization of the S_1 energy results in a twisting of the phenolic and benzotriazolic rings as well as in a pyramidization at the N_2 atom. At $\theta(C_2'C_1'N_2N3) \approx 60°$, the CC2 iteration cycle ceases to converge. An analysis of the data reveals that the reason is the vanishing of the S_1–S_0 energy gap. This result strongly suggests that there exists a conical intersection between the S_1 and S_0 surfaces near the minimum of the excited state. Since this topographical feature of the energy surfaces cannot be characterized at the CC2 level, we have performed a CASSCF search for the conical intersection starting from the CC2 initial guess. The resulting structure is shown in Figure 1d (Cartesian geometry in the Supporting Information).

It is seen that at the S_1–S_0 conical intersection the phenyl and benzotriazole rings are almost perpendicular to each other. The relevant dihedral angles are $\theta(C_2'C_1'N_2N_3) = 58.3°$, and $\theta(C_2'C_1'N_2N_1) = -77.3°$. The sum of the bond angles at the N_2 and N_3 atoms is 344.7 and 318.0°, respectively, indicating a significant perturbation of the sp^2 hybridization, in particular of the latter N atom.

3.3. Potential-Energy Profiles. The PE profiles calculated along the minimum-energy paths for hydrogen transfer (OH bond length) and inter-ring twisting coordinate ($C_2'C_1'N_2N_3$ dihedral angle) of the enol and keto tautomers in the S_0 and S_1 states are shown in Figure 2 (full curves). The profiles were obtained by calculating the CC2/cc-pVDZ energy of the S_0 and S_1 states at their MP2/SV(P) and CC2/SV(P) optimized geometries, respectively. In addition, the "vertical" PE profiles of a given state, calculated at the optimized geometry of the other state, have been determined (dashed curves). Here $S_1^{(S_1)}$ denotes the energy of the S_1 state calculated along the reaction path optimized in the S_1 state, $S_1^{(S_0)}$ denotes the energy of the S_1 state calculated along the reaction path optimized in the S_0 state, etc.

The $S_0^{(S_0)}$ curve in Figure 2a exhibits the barrier for ring torsion of the enol form in the S_0 state (≈ 0.41 eV). The energy profile of the S_1 state calculated along the S_0 reaction path ($S_1^{(S_0)}$ in Figure 2a) indicates a significant increase of this barrier (≈ 1.3 eV) in the S_1 state. Unfortunately, only the optimization of the perpendicular conformer of the enol form (C_s symmetry) was possible in the S_1 state. Any distortion of this conformation which breaks the C_s symmetry results in a spontaneous transfer of the proton and in the formation of the keto tautomeric form.

The energy profiles along the hydrogen-transfer reaction path are displayed in Figure 2b. As expected, the hydrogen transfer reaction is endothermic in the ground state, but exothermic in the first excited singlet state. In both cases, the energy profile is barrierless. The planar keto-type S_1 structure (the S_1' state) lies 3.21 eV above the global minimum of the ground state (see Table 1). The fluorescence is strongly allowed ($f = 0.32$) and would have a center wavelength of about 600 nm (2.04 eV) if it could be observed in the gas phase. As mentioned above, the S_1' state is unstable with respect to out-of-plane deformation. Unconstrained optimization of the S_1' state results in twisting and leads to the conical intersection of the S_1 surface with the S_0 surface. This instability of the S_1' state explains the extremely low quantum yield of fluorescence of TIN—P ($\Phi \approx 10^{-5}$) observed in condensed phases,[6,7] despite the large transition dipole moment of the S_1—S_0 radiative transition.
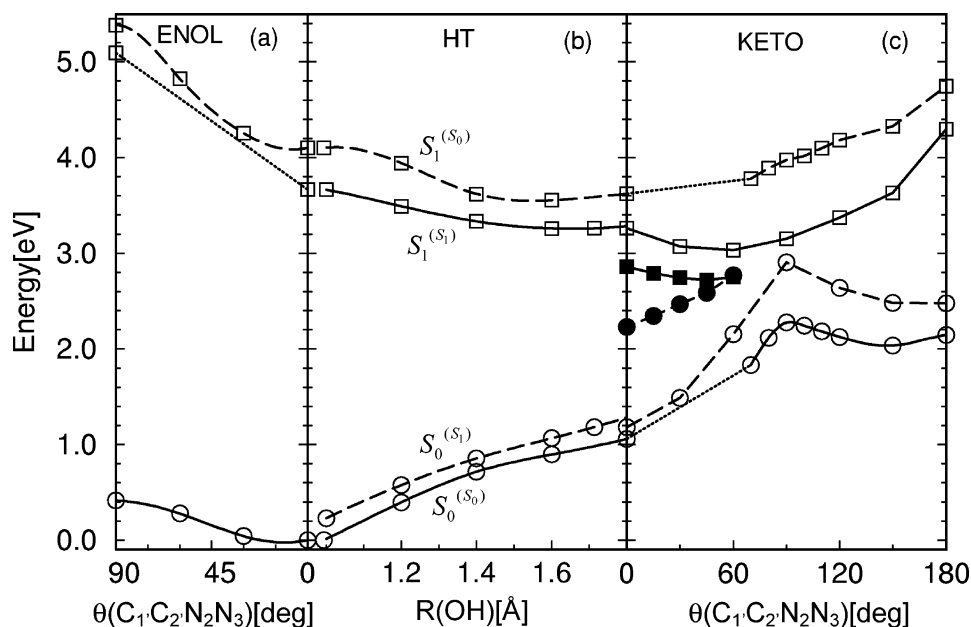
Figure 2. CC2/cc-pVDZ energy profiles of the S_0 state (circles) and S_1 state (squares) as a function of the torsional reaction path (a, c) and the hydrogen transfer reaction path (b). Full lines: energy profiles of reaction paths determined in the same electronic state ($S_0^{(S_0)}$, $S_1^{(S_1)}$). Dashed lines: energy profiles of reaction paths determined in the complementary electronic state ($S_0^{(S_1)}$, $S_1^{(S_0)}$). The dotted lines denote interpolations where reaction-path optimizations were not possible. In part c, open symbols correspond to twisting in the S_1 state without pyramidization at N_2, filled symbols correspond to the reaction path with inclusion of pyramidization at N_2.
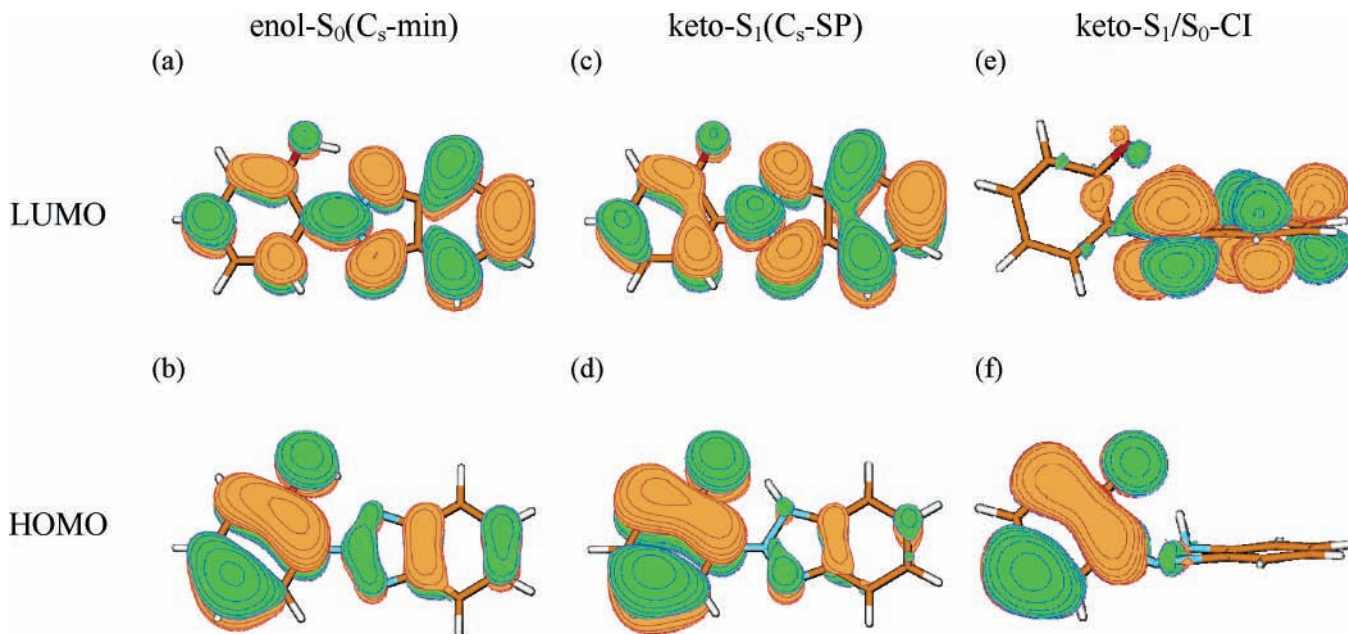

Figure 3. Highest occupied (HOMO) and the lowest unoccupied (LUMO) Hartree−Fock molecular orbitals of TIN−H, determined at the equilibrium geometry of the electronic ground state (a, b), at the C_s-equilibrium geometry of the S_1 state (c, d) and at the CASSCF conical intersection of the S_1 and S_0 states (e, f). The colors green/yellow encode the sign of the wave function.

To visualize the character of the potential-energy surfaces with respect to out-of-plane deformation, Figure 2c shows the energy profiles for the twisting reaction path (the $C_2'C_1'N_2N_3$ dihedral angle). The $S_0^{(S_0)}$ curve clearly reveals the local minimum corresponding to the open keto conformer (Figure 1b). We were able to optimize the minimum-energy path in the ground state from this local minimum through the saddle point down to $\theta(C_2'C_1'N_2N_3) = 70°$. Below this value, a spontaneous hydrogen transfer takes place, resulting in the formation of the enol tautomer. This part of the PE function is represented by the dotted line in Figure 2c. The energy profile of the S_1 state calculated along the ground-state reaction path, $S_1^{(S_0)}$, is a barrierless function of the dihedral angle, sloped in the direction of the enol form.

To provide more insight into the nature of the internal coordinates involved in the stabilization of the S_1 state due to out-of-plane deformation, the energy profiles of two minimum-energy reaction paths calculated in the S_1 state are shown in Figure 2c. The first path, denoted by open symbols (circles for S_0, squares for S_1), describes pure twisting (without pyramidization at the N_2 nitrogen) around the $C_1'N_2$ bond and involves a concerted change of the $C_2'C_1'N_2N_3$ and $C_2'C_1'N_2N_1$ dihedral angles (all remaining internal coordinates are optimized, of course). The second path, denoted by filled symbols in Figure

Photophysics of Organic Photostabilizers

J. Phys. Chem. A, Vol. 110, No. 19, 2006 **6305**

2c, was obtained by taking the $C_2'C_1'N_2N_3$ dihedral angle as the driving coordinate and optimizing all remaining internal coordinates, including the $C_2'C_1'N_2N_1$ dihedral angle. The latter reaction path allows pyramidization at the N_2 nitrogen.

It can be seen (Figure 2c) that pure twisting around the $C_1'N_2$ bond (without pyramidization at the N_2 nitrogen) results in a stabilization of the S_1 state by about 0.23 eV with respect to the planar structure. The S_0 energy (circles) approaches the S_1 energy (squares) from below, but an energy gap of about 0.25 eV remains at the closest approach of these states (for perpendicular conformation of the rings). The reaction path which allows pyramidization at the N_2 nitrogen (solid symbols in Figure 2c), on the other hand, leads directly to the S_1–S_0 intersection at $\theta(C_2'C_1'N_2N_3) \approx 60°$. The S_1 potential-energy profiles calculated along the two reaction paths are parallel to each other, the latter profile being lower in energy by about 0.3 eV. This stabilization energy of the S_1 state results from the pyramidization at the N_2 nitrogen. It is interesting to notice that the energy of the S_1–S_0 intersection obtained in the unconstrained CC2 optimization of the S_1 state is by about 0.4 eV lower than the CC2 energy obtained at the CASSCF-optimized conical intersection (Table 1). This result stresses importance of dynamical electron correlation effect for optimization of the excited-state geometry.

To provide insight into the electronic structure of the states involved in the photophysics of TIN–H, we display in Figure 3 the highest occupied (HO) and lowest unoccupied (LU) molecular (MO) orbital, which are singly occupied in the S_1 state, at the planar S_0 equilibrium geometry (a, b), the planar S_1 keto configuration (c, d) and at the perpendicular geometry of the S_1–S_0 conical intersection (e, f). It is seen that only π orbitals of the aromatic rings are involved as frontier orbitals. It can further be seen that the $S_0 \rightarrow S_1$ excitation at the S_0 equilibrium geometry is accompanied by a moderate shift of electron density from the phenyl ring to the benzotriazol system. At the S_1' conformation, the ground state is highly polar (see Table 1) due to the nearly complete localization of the HOMO on the phenolic ring (Figure 3d), while the proton has been transferred to the benzotriazole ring. This polarity is reduced in the S_1' state due to the delocalized character of the LUMO (Figure 3c). At the configuration of the S_1–S_0 conical intersection, the HOMO and LUMO are completely localized on the phenolic and benzotriazole moieties, respectively (Figure 3e,f). TIN–H at this configuration thus is an almost perfect biradical, as is typical for a degeneracy of the open-shell S_1 state with the closed-shell ground state.[41]

Summarizing this section, we can state that we have identified three nuclear coordinates which play the principal roles in the relaxation from the Franck–Condon area of the S_1 potential-energy surface toward the intersection with the ground-state surface. These are as follows: OH stretching (0.41 eV stabilization energy), twisting around the $C_1'N_2$ bond ($\Delta E = 0.23$ eV), and pyramidization at the N_2 atom ($\Delta E = 0.28$ eV). The rest of stabilization energy ($\Delta E = 0.35$ eV) results from the relaxation of the remaining coordinates along the reaction path from the ground-state equilibrium geometry to the S_1–S_0 intersection. The minimum-energy path on the S_1 surface leads in a barrierless way from the FC geometry of the system to the conical intersection with the ground state, the reaction being exothermic by about 1.27 eV. These features of the potential-energy surface of the lowest excited singlet state of TIN–H have important consequences for photophysics of the system.

4. Conclusions

The computational results suggest the following qualitative global picture of the photophysics of TIN. The primary excited-state process certainly is hydrogen transfer. This reaction is barrierless (see Figure 2b) and thus extremely fast. Previous kinetic measurements have established time constants of the order of a few tens of femtoseconds for barrierless excited-state proton-transfer reactions.[42–44] This conclusion is in agreement with the observations of ref 13 for TIN–P. The planar S_1 keto-type conformation (S_1') is unstable with respect to twisting (see Figure 2c). The twisting breaks the O···H–N intramolecular hydrogen bond of S_1' and leads, accompanied by a moderate pyramidization at N_2, on a barrierless reaction path to the S_1–S_0 conical intersection (see Figure 2c). At the S_1–S_0 conical intersection, the system switches from the S_1 surface to the S_0 surface via a nonadiabatic trasition. Experimental data for similar systems as well as theoretical studies for related models[45,46] indicate that the nonradiative transition can occur within a fraction of a torsional period. In the S_0 state, the enol-type O–H···N hydrogen bond is re-formed (Figure 2b). This bond and the torsional potential in the S_0 state (Figure 2a) steer the system back to the planar S_0 conformation. This essential role of twisting in the internal-conversion process of TIN explains the pronounced temperature dependence of the nonradiative decay rate in low-temperature organic glasses as well as the effect of pretwisting of the electronic ground state, in full accord with the interpretations of refs 15 and 16.

An interesting finding of the calculations is the existence of an open keto-type local minimum on the S_0 energy surface (see Figure 2c) about 2 eV (46 kcal/mol) above the closed enol-type global minimum. The barrier height of 5.5 kcal/mol separating the minima (see section 3.1) allows, in principle, the trapping of the system in the open keto-type tautomer. This would result in production of a photochromic species since this tautomeric form absorbs strongly in the red (see Table 1). On the other hand, the barrier is low compared with the excess energy available after the $S_0 \rightarrow S_1$ internal conversion process. It is thus plausible that the global minimum structure of TIN is restored with a probability very close to unity, which is a requirement for the function of TIN as an effective photostabilizer. This result indicates that the photochromism of certain ESIHT systems (e.g., HBO or HBT) is related to the conical intersection between the potential-energy surfaces of the S_0 and S_1 states.

A more quantitative description of the photocycle of TIN requires the treatment of the photoinduced dynamics by quantum wave packet or quasiclassical trajectory calculations. The present results, together with previous ab initio calculations on related systems,[21,23] have revealed the most relevant electronic states and nuclear degrees of freedom involved in the photophysics of hydroyphenyl–benzotriazole photostabilizers, which are prerequisites for accurate quantum dynamics calculations.

Supporting Information Available: Tables of the Cartesian geometry parameters of the structures. This material is available free of charge via the Internet at http://pubs.acs.org.

References and Notes

(1) Heller, H. J.; Blattmann, H. R. *Pure Appl. Chem.* **1972**, *30*, 145.
(2) Allen, N. S. *Polym. Photochem.* **1983**, *3*, 167.

(3) Woessner, G.; Goeller, G.; Kollat, P.; Stezowski, J. J.; Hauser, M.; Klein, U.K.A.; Kramer, H. E. A. *J. Phys. Chem.* **1984**, *88*, 5544.

(4) Woessner, G.; Goeller, G.; Rieker, J.; Hoier, H.; Stezowski, J. J.; Daltrozzo, E.; Neureiter, M.; Kramer, H. E. A. *J. Phys. Chem.* **1985**, *89*, 3629.

(5) Goeller, G.; Rieker, J.; Maier, A.; Stezowski, J. J.; Daltrozzo, E.; Neureiter, M.; Port, H.; Wiechmann, M.; Kramer, H. E. A. *J. Phys. Chem.* **1988**, *92*, 1452.

(6) Formosinho, S. J.; Arnaut, L. G. *J. Photochem. Photobiol.* **1993**, *75*, 21.

(7) Orsom, S. M.; Brown, R. G. *Prog. React. Kinet.* **1994**, *19*, 45.

(8) Rieker, J.; Lemmert-Schmidt, E.; Goeller, G.; Roessler, M.; Stueber, G. J.; Schettler, H.; Kramer, H. E. A.; Stezowski, J. J.; Hoier, H.; Henkel, S.; Schmidt, A.; Port, H.; Wiechmann, M.; Rody, J.; Rytz, G.; Slongo, M.; Birbaum, J.-L. *J. Phys. Chem.* **1992**, *96*, 10225.

(9) Catalan, J.; Fabero, F.; Guijarro, M. S.; Claramunt, R. M.; Santa Maria, M. D.; de la Concepcion, M.; Cano, F. H.; Elguero, J.; Sastre, R. *J. Am. Chem. Soc.* **1990**, *112*, 747.

(10) Wiechmann, M.; Port, H.; Laermer, F.; Frey, W.; Elsaesser, T. *Chem. Phys. Lett.* **1990**, *165*, 28.

(11) Wiechmann, M.; Port, H.; Frey, W.; Laermer, F.; Elsaesser, T. *J. Phys. Chem.* **1991**, *95*, 1918.

(12) Frey, W.; Elsaesser, T. *Chem. Phys. Lett.* **1992**, *189*, 565.

(13) Chudoba, C.; Lutgen, S.; Jentzsch, T.; Riedle, E.; Woerner, M.; Elsaesser, T. *Chem. Phys. Lett.* **1995**, *240*, 35.

(14) Otterstedt, J.-E. A. *J. Chem. Phys.* **1973**, *58*, 5716.

(15) Flom, S. R.; Barbara, P. F. *Chem. Phys. Lett.* **1983**, *94*, 488.

(16) Maliakal, A.; Lem, G.; Turro, N. J.; Ravichandran, R.; Suhadolnik, J. C.; De Bellis, A. D.; Wood, M. G.; Lau, J. *J. Phys. Chem. A* **2002**, *106*, 7680.

(17) Kozich, V.; Dreyer, J.; Werncke, W. *Chem. Phys. Lett.* **2004**, *399*, 484.

(18) Sobolewski, A. L.; Domcke, W. In *The Reaction Path in Chemistry;* Heidrich, D., Ed.; Kluwer Academic: Dordrecht, The Netherlands, 1995; p 257.

(19) Scheiner, S. *J. Phys. Chem. A*, **2000**, *104*, 5898.

(20) Catalan, J.; de Paz, J. L. G.; Torres, M. R.; Tornero, J. D. *J. Chem. Soc., Faraday Trans.* **1997**, *93*, 1691.

(21) Estevez, C. M.; Bach, R. D.; Hass, K. C.; Schneider, W. F. *J. Am. Chem. Soc.* **1997**, *119*, 5445.

(22) Domcke, W.; Yarkony, D. R.; Köppel, H., Eds.; *Conical Intersections: Electronic Structure, Dynamics and Spectroscopy*; World Scientific: Singapore, 2004.

(23) Paterson, M. J.; Robb, M. A.; Blancafort, L.; De Bellis, A. D. *J. Am. Chem. Soc.* **2004**, *126*, 2912.

(24) Kato, S. *J. Chem. Phys.* **1988**, *88*, 3045.

(25) Sobolewski, A. L.; Domcke, W. *Chem. Phys. Lett.* **1991**, *180*, 381.

(26) Sobolewski, A. L.; Woywod, C.; Domcke, W. *J. Chem. Phys.* **1993**, *98*, 5627.

(27) Palmer, I. J.; Ragazos, I. N.; Bernardi, F.; Olivucci, M.; Robb, M. A. *J. Am. Chem. Soc.* **1993**, *115*, 673.

(28) Sobolewski, A. L.; Domcke, W. *Chem. Phys.* **1994**, *184*, 114.

(29) Matsika, S. *J. Phys. Chem. A* **2004**, *108*, 7584.

(30) Tomic, K.; Tatchen, J.; Marian, C. M. *J. Phys. Chem. A* **2005**, *109*, 8410.

(31) Christiansen, O.; Koch, H.; Jørgensen, P. *Chem. Phys. Lett.* **1995**, *243*, 409.

(32) Hättig, C.; Weigend, F. *J. Chem. Phys.* **2000**, *113*, 5154.

(33) Hättig, C. *J. Chem. Phys.* **2003**, *118*, 7751.

(34) Köhn, A.; Hättig, C. *J. Chem. Phys.* **2003**, *119*, 5021.

(35) Ahlrichs, R.; Bär, M.; Häser, M.; Horn, H.; Kölmel, C. *Chem. Phys. Lett.* **1989**, *162*, 165.

(36) Schaefer, A.; Horn, H.; Ahlrichs, R. *J. Chem. Phys.* **1992**, *97*, 2571.

(37) Aquino, A. J. A.; Lischka, H.; Hättig, C. *J. Phys. Chem. A* **2005**, *109*, 3201.

(38) GAUSSIAN 98, Gaussian, Inc. Pittsburgh, PA, 1998.

(39) Weigend, F.; Häser, M.; Patzelt, H.; Ahlrichs, R. *Chem. Phys. Lett.* **1998**, *294*, 143.

(40) Woon, D. E.; Dunning, T. H., Jr. *J. Chem. Phys.* **1993**, *98*, 1358.

(41) Klessinger, M.; Michl, J. *Excited States and Photochemistry of Organic Molecules*, VCH: Weinheim, Germany, 1995; Section 4.3.

(42) Herek, J. L.; Pedersen, S.; Banares, L.; Zewail, A. H. *J. Chem. Phys.* **1992**, *97*, 9046.

(43) Lochbrunner, S.; Schultz, T.; Schmitt, M.; Shaffer, J. P.; Zgierski, M. Z.; Stolow, A. *J. Chem. Phys.* **2001**, *114*, 2519.

(44) Stock, K.; Biziak, T.; Lochbrunner, S. *Chem. Phys. Lett.* **2002**, *354*, 409.

(45) Seidner, L.; Domcke, W. *Chem. Phys.* **1994**, *186*, 27.

(46) See ref 22, Chapter 9.